Effect of kinetic ions on the toroidal double-tearing modes

Ruibo Zhang(张睿博)[1,2], Lei Ye(叶磊)[1,†], Yang Chen[3], Nong Xiang(项农)[1], and Xiaoqing Yang(杨小庆)[1]

[1] *Hefei Institutes of Physical Science, Chinese Academy of Sciences, Hefei* 230031, *China*
[2] *University of Science and Technology of China, Hefei* 230026, *China*
[3] *Center for Integrated Plasma Studies, University of Colorado at Boulder, Boulder, Colorado* 80309, *USA*

(Received 7 April 2022; revised manuscript received 27 June 2022; accepted manuscript online 8 July 2022)

We investigate the effects of kinetic ions on double-tearing modes (DTMs) using the gyrokinetic particle-in-cell simulation code GEM with a gyrokinetic ion/fluid electron hybrid model. It is found that the ion kinetic effects can decrease the growth rate of the DTMs. This effect is more significant for stronger coupling of DTMs with smaller distance between the rational surfaces. Kinetic ions can also enhance the coupling effect between the two rational surfaces. Energy transfer analyses between particles and wave fields show that the stabilizing effect of kinetic ions comes mainly from the perpendicular magnetic drift of ions in the coupling region and around the outer rational surface.

Keywords: double-tearing modes, kinetic ions, coupling effect

PACS: 52.35.Py, 52.65.Tt, 52.35.Mw **DOI:** 10.1088/1674-1056/ac7f89

1. Introduction

Double-tearing modes (DTMs) can be excited in a reversed magnetic shear configuration, due to the two rational surfaces with the same helicity. Different from the single-tearing mode (STM), the two tearing modes on neighboring rational surfaces can be coupled with each other and the linear growth rate of the DTMs is much larger than that of the STM. In a slab plasma, the resistivity scaling of the DTMs ($\gamma \sim \eta^{1/3}$)[1] is weaker than that of the STM ($\gamma \sim \eta^{3/5}$).[2] Here γ and η are the growth rate of the tearing mode and the resistivity, respectively. Moreover, nonlinear DTMs can generate strong sheared flows, release large bursts of kinetic energy, and cause the off-axis sawtooth crashes,[3] which may give rise to a major disruption. Therefore, it is important to understand the mechanism of DTMs and to develop methods to suppress the DTMs in tokamaks. Since DTMs are formed by the coupling of tearing modes to each other on two rational surfaces, it is natural to anticipate that the DTM instability can be mitigated by either suppressing or decoupling the tearing modes on two rational surfaces. It has been found that toroidicity[4,5] has stabilizing effects on the STM. On the other hand, shear flows,[6–10] diamagnetic effects[11,12] and external current drives[13,14] can help to decouple the two rational surfaces in a DTM.

It is difficult to analytically predict behaviors of the tearing mode due to its multi-scale property, and the kinetic effects of ions near the tearing layer may be important. In the past few years, many theoretical and numerical investigations have pointed out that kinetic ions are important in evolution of the STM.[15–20] Theoretical analyses and numerical simulations found that trapped energetic ions have a stabilizing effect on DTMs.[21,22] An investigation of the kinetic ions effect on DTMs has been carried out with the gyrokinetic code GTC. It was found that the kinetic ions destabilize the DTMs in toroidal geometry without toroidal coupling.[23] With energetic ions, the off-axis sawtooth oscillations induced by DTMs were observed in the TFTR,[3] CHS[24] and HL-2A[25] experiments.

In our previous work,[5] the gyrokinetic particle-in-cell code GEM was employed to study the toroidal effects and kinetic ion effects on STM with the hybrid gyrokinetic ion/fluid electron model. A new field solver in toroidal geometry has been developed for the simulation of low-n modes in tokamaks. It was found that kinetic ions, mainly the passing particles, have a stabilizing effect on the STM. In the present study, we continue to investigate the DTMs in tokamak geometry using GEM. The main focus is on the the influence of kinetic ions on the coupling of DTMs between the two rational surfaces.

The remaining part of this paper is organized as follows. The simulation model and basic equations are briefly described in Section 2. The effects of kinetic ions on the DTMs are studied in Section 3. The conclusion is drawn in Section 4.

2. Physical model

The gyrokinetic ion/fluid electron hybrid model is employed in this paper to study the $(m = 3, n = 1)$ DTMs in the toroidal geometry. In the hybrid model, the ions are described by the gyrokinetic equation, the particle trapping and the finite-orbit-width effects are included. The electrons are treated as a massless isothermal fluid. Recently, the hybrid version of GEM has been extended to low-n modes by devel-

†Corresponding author. E-mail: lye@ipp.ac.cn

© 2023 Chinese Physical Society and IOP Publishing Ltd

oping a new field solver, and applied to the simulation of the $(2,1)$ STM in toroidal geometry.[5] Here for convenience we give a brief description of the fluid model for electrons. More details can be found in Refs. [5,26,27] and references therein.

The electron continuity equation is written as

$$\frac{\partial \delta n_{\rm e}}{\partial t}+\boldsymbol{B}\cdot\nabla\frac{n_0\delta u_{\parallel {\rm e}}}{B}+\delta\boldsymbol{B}_\perp\cdot\nabla\frac{n_0 u_{\parallel {\rm e}0}}{B}+\delta\boldsymbol{B}_\perp\cdot\nabla\frac{n_0\delta u_{\parallel {\rm e}}}{B}$$
$$+\boldsymbol{v}_E\cdot\nabla(n_0+\delta n_{\rm e})+\frac{1}{m_{\rm e}\Omega_{\rm e}B^2}\boldsymbol{B}\times\nabla B\cdot\nabla\left(\delta p_{{\rm e}\perp}+\delta p_{{\rm e}\parallel}\right)$$
$$+\frac{2n_0}{B^3}\boldsymbol{B}\times\nabla B\cdot\nabla\phi=0, \tag{1}$$

with $u_{\parallel {\rm e}0}$ and $\delta u_{\parallel {\rm e}}$ being the equilibrium electron parallel flow and the perturbed electron parallel flow, respectively. The perturbed electron pressure is $\delta p_{{\rm e}\perp}=\delta p_{{\rm e}\parallel}=n_{\rm e}\delta T_{\rm e}+T_{\rm e}\delta n_{\rm e}$, $\delta T_{\rm e}$ and $\delta n_{\rm e}$ are perturbed electron temperature and perturbed electron density, respectively. The last two terms on the left-hand side of Eq. (1) are associated to the toroidal geometry. The toroidal pressure term $\nabla(\delta p_{{\rm e}\perp}+\delta p_{{\rm e}\parallel})$ arises from the guiding-center magnetic drift in a low-β plasma,[28] and the last term from the compressibility of the $\boldsymbol{E}\times\boldsymbol{B}$ drift.

The parallel vector potential $A_\parallel$ can be evolved by

$$\frac{\partial A_\parallel}{\partial t}=E_\parallel-\nabla_\parallel\phi. \tag{2}$$

The Ohm law is simplified to

$$E_\parallel=\eta j_\parallel, \tag{3}$$

with $j_\parallel=\delta j_{\parallel {\rm i}}-en_0\delta u_{\parallel {\rm e}}$ being the parallel perturbed current. The parallel ion current $\delta j_{\parallel {\rm i}}$ is calculated from the ion distribution function.

The electron parallel flow velocity $\delta u_{\parallel {\rm e}}$ used in the electron continuity equation, i.e., Eq. (1), is obtained from Ampere's equation

$$en_0\delta u_{\parallel {\rm e}}=\delta j_{\parallel {\rm i}}+\frac{1}{\beta_{\rm u}}\nabla_\perp^2 A_\parallel. \tag{4}$$

The vorticity equation derived by the quasi-neutral equation can be transformed to

$$-\nabla_\perp^2\frac{\partial\phi}{\partial t}=\frac{q}{mn_0}\left(B^2-\frac{mT}{q^2}\nabla_\perp^2\right)\frac{\partial}{\partial t}\left(q_{\rm i}\delta n_{\rm i}-e\delta n_{\rm e}\right) \tag{5}$$

using the Padé approximation. The second term on the right-hand side of Eq. (5) indicates the finite-Larmor-radius (FLR) effect.

The main closure relation for this fluid electron model is the linearized isothermal condition for the perturbed electron temperature,[29]

$$\boldsymbol{b}\cdot\nabla\delta T_{\rm e}+\frac{\delta\boldsymbol{B}_\perp}{B}\cdot\nabla T_{\rm e}=0. \tag{6}$$

This isothermal condition is derived from the electron drift kinetic equation by assuming $\omega\ll k_\parallel v_{\rm Te}$, where ω is the characteristic frequency of the fluctuations, $v_{\rm Te}$ is the electron thermal speed, and $k_\parallel$ is the parallel wave number. The coupling effect of different poloidal harmonics in toroidal geometry is preserved in all the following simulations.

3. Simulation results

In this section, the $(m,n)=(3,1)$ DTMs in a tokamak plasma are studied by gyrokientic particle-in-cell (PIC) simulation. A magnetic equilibrium with concentric circular flux-surfaces is used, with an on-axis magnetic field $B_0=1.6$ T, major radius $R_0=1.82$ m and inverse aspect ratio $\varepsilon=a/R_0=0.25$, where $a=0.46$ m is the minor radius. The safety factor profile is set as

$$q(r)=q_{\rm c}\left[1+\left(\frac{r/a}{r_0}\right)^{2\lambda}\right]\left[1+A\exp\left(-\left(\frac{r/a}{\delta}\right)^2\right)\right], \tag{7}$$

with $\lambda=1$, $r_0=0.412$, $\delta=0.303$, $A=3$, and $q_{\rm c}$ is varied for different separations ($d_{\rm s}$) of the two $q=3$ rational surfaces, as shown in Fig. 1. The density profile is set to be constant as $n_{0{\rm i}}=n_{0{\rm e}}=1.3\times10^{19}$ m^{-3}. The temperature profiles are $T_{\rm e}(r)=-T_{0{\rm e}}(r/a-0.45)+T_{0{\rm e}}$ and $T_{\rm i}(r)=-T_{0{\rm i}}(r/a-0.45)+T_{0{\rm i}}$ for electrons and ions. The $T_{0{\rm e}}=0.1$ keV is fixed. $T_{0{\rm i}}$ can be varied to study the effect of a finite ion temperature. In the following the resistivity η and the growth rate γ are normalized to $\eta_0=B_0/en_{0{\rm e}}=0.77\ \Omega$m and $\omega_{\rm c}=eB_0/m_{\rm i}=7.74\times10^7$ Hz, respectively.

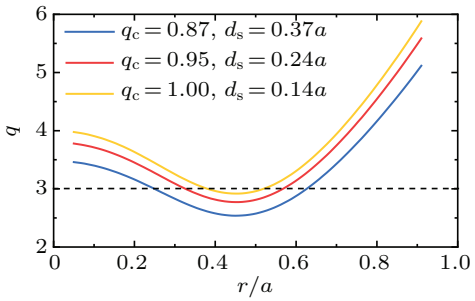


Fig. 1. Safety factor profiles for different $d_{\rm s}$ by varying $q_{\rm c}$.

3.1. Simulations of DTMs with cold ions

Firstly, we present the simulation result for the DTMs with cold ions ($T_{0{\rm i}}=10^{-3}$ keV and $L_{\rm Ti}^{-1}=0$), where the kinetic effects of ions are in fact excluded. Figure 2 shows the typical 2D mode structure of DTMs for the perturbed electric potential $\delta\phi$ and perturbed vector potential $\delta A_\parallel$ on the poloidal cross section with $\eta=2\times10^{-5}$. It can be observed that the mode structure has an in-out asymmetry due to the toroidal magnetic field.

As we know, the separation of the two rational surfaces is a key factor affecting the coupling effect between the two rational surfaces. Thus, several simulations have been performed with different $d_{\rm s}$ and the corresponding radial mode structures of $\delta\phi$ are plotted in Fig. 3. It can be seen that for a larger separation of $d_{\rm s}=0.37a$, the mode structure can be considered as a simple superposition of the two STMs located

on each rational surface, respectively. However, as d_s is decreased, the coupling effect between the two rational surfaces is stronger, and the mode amplitude in the coupling region can be significantly increased. The variation of radial modes structure between the two rational surfaces can also be used as a criterion for the coupling effect of the DTMs.

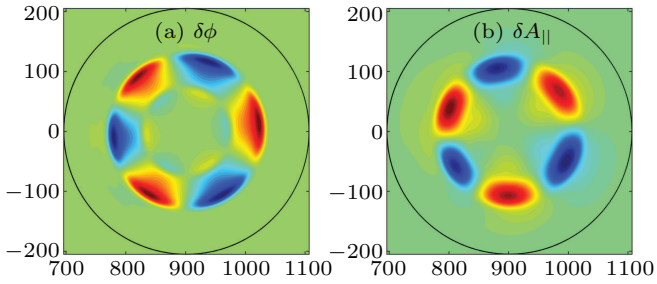


Fig. 2. Mode structure of DTMs with $\varepsilon = 0.25$ and $\eta = 2 \times 10^{-5}$.

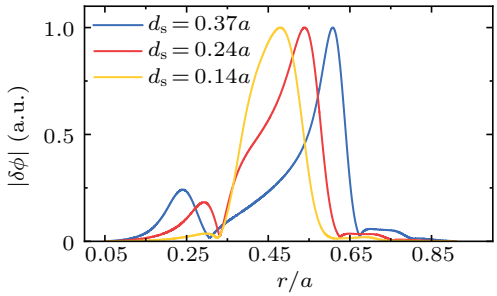


Fig. 3. The radial mode structures of $\delta\phi$ for $d_s = 0.37a$, $d_s = 0.24a$ and $d_s = 0.14a$ for $\eta = 2 \times 10^{-5}$ with $T_{0i} = 1 \times 10^{-3}$ keV. All the profiles are normalized to the their maximum absolute values. The mode amplitude in the coupling region is increased by decreasing d_s.

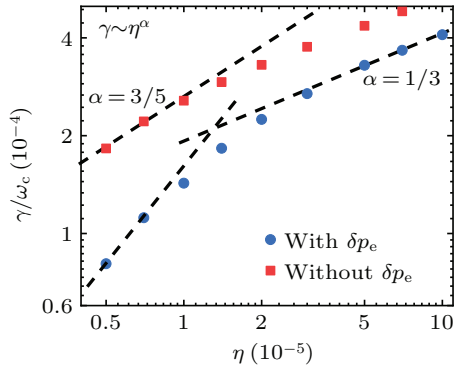


Fig. 4. The dependence of growth rate on η with and without toroidal pressure term.

For given $d_s = 0.24a$, the growth rate of the DTMs for different η is shown in Fig. 4. Two resistivity scalings, $\gamma \sim \eta^{0.9}$ and $\gamma \sim \eta^{1/3}$ can be found in the small and large resistivity limit, respectively. The scaling for large η is consistent with the DTM scaling, which is also consistent with the numerical results presented in Refs. [22,30]. However, the scaling for small is larger than that of the STM ($\gamma \sim \eta^{3/5}$). We find that this discrepancy is associated with the toroidal effect, specifically the electron toroidal pressure term δp_e in Eq. (1). This term arises from the guiding-center magnetic drift in a toroidal magnetic field. As plotted by red squares in Fig. 4, when the toroidal pressure term is neglected in the simulation, the scaling of STM($\gamma \sim \eta^{3/5}$) is recovered in small η limit.

The mode structure of DTMs also changes with η. Figure 5 shows the radial structures of $\delta\phi$ for three different value of η. It can be seen that the mode amplitude in the coupling region increases with η. Similar results have been shown in Fig. 3, where the enhanced coupling is induced by decreasing d_s. Nevertheless, for a fixed separation of the two rational surfaces d_s, the width of the STM on each rational surface can be broadened by increasing η. Therefore, the interaction between the two modes can also be enhanced. This process is also consistent with the different resistivity scalings in two η limits, as shown in Fig. 4.

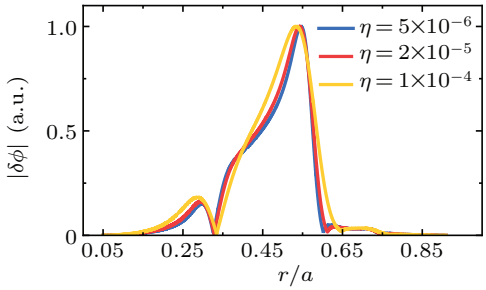


Fig. 5. The radial mode structures for $\eta = 5 \times 10^{-6}$, $\eta = 2 \times 10^{-5}$ and $\eta = 1 \times 10^{-4}$ with $T_{0i} = 1 \times 10^{-3}$ keV. All the profiles are normalized to the their maximum absolute values. The mode amplitude in the coupling region is increased with η.

3.2. Effect of kinetic ions on the DTMs

In this subsection, the kinetic effects of thermal ions on the DTMs are investigated numerically. Firstly, the dependence of the growth rates of the DTMs on η for cold and thermal ions are compared in Fig. 6. It can be seen that the growth rate of the DTMs can be effectively reduced by thermal ions, the suppression effect increases with η. Moreover, with thermal ions, the DTMs scaling, $\gamma \sim \eta^{1/3}$, can be extended to smaller resistivity of $\eta \approx 1 \times 10^{-5}$. This modification to the resistivity scaling indicates an enhanced coupling of DTMs between the two rational surfaces induced by thermal ions.

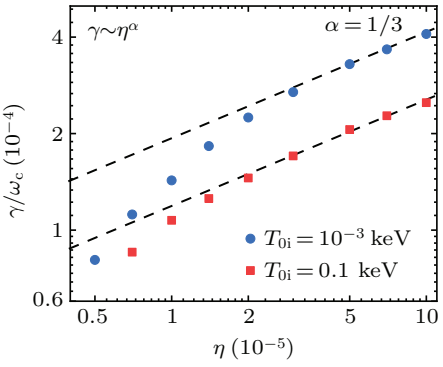


Fig. 6. The dependence of growth rate on η for cold ($T_{0i} = 1 \times 10^{-3}$ keV) and thermal ($T_{0i} = 0.1$ keV) ions with $L_{Ti}^{-1} = 0$. It can be seen that the growth rate of the DTMs can be effectively suppressed by thermal ions and the suppression effect increases with η.

The effect of ion temperature on the growth rate and frequency of the DTMs are also studied and plotted in Fig. 7. It

can be seen that the growth rate decreases as T_{0i} increases. For the frequency of the DTMs, there exists a threshold for T_{0i}. When $T_{0i} < T_{0e}$, the frequency increases with the increase of T_{0i}, when $T_{0i} > T_{0e}$, the frequency decreases with the increase of T_{0i}.

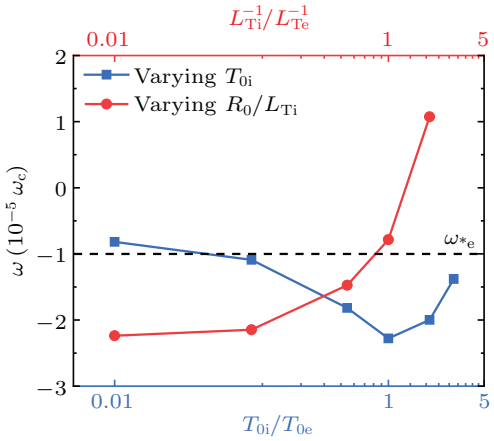


Fig. 7. The dependence of growth rate and frequency on T_{0i}.

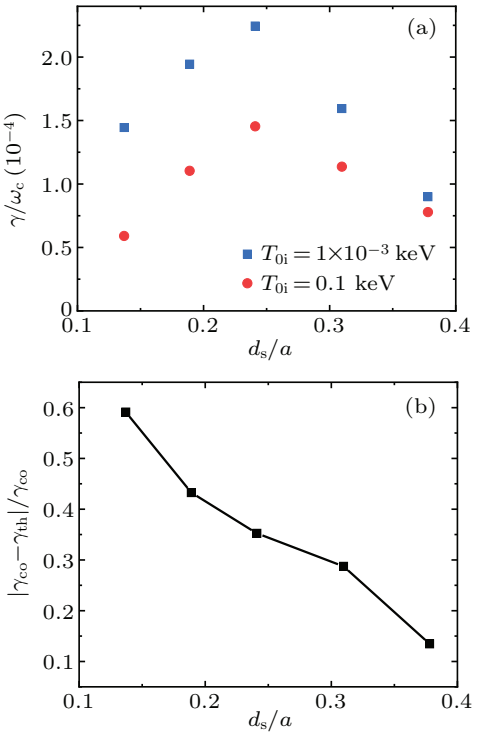


Fig. 8. (a) The growth rate of DTMs for cold and thermal ions for different d_s. (b) The stabilization effect of kinetic ions decreases as d_s increases. The superscripts 'co' and 'th' represent cold and thermal ions, respectively.

To further illustrate the effect of thermal ions on the DTMs, especially the coupling effect between the two rational surfaces, the simulations of the DTMs with different separations of the two rational surfaces are carried out. The simulation results for the growth rate are plotted in Fig. 8. From Fig. 8(a), it can be found that with d_s increasing, the growth rate increases at first and then decreases, which is independent of ion temperature. In Fig. 8(b), it can be seen that the stabilization effect of thermal ions decreases as d_s increases. As we have shown before, the coupling effect can be enhanced as d_s decreases. This indicates that the stabilization effect of thermal ions on DTMs depends on the the coupling effect between the two rational surfaces. In Fig. 9, the radial mode structures of the DTMs for different d_s with cold and thermal ions are plotted. It can be seen that when d_s is large ($d_s > 0.24a$), the coupling effect between the two rational surfaces is weak, thermal ions can increase the mode amplitude in the coupling region. This enhancement effect increases with the coupling effect. When d_s is small ($d_s > 0.24a$), the coupling effect is strong and the resistivity scaling is $\gamma \sim \eta^{1/3}$, the coupling enhancement effect of thermal ions becomes weaker.

The above results suggest that thermal ions can suppress the growth of the DTMs. The suppression effect of kinetic ions becomes stronger with the enhancement of the coupling between rational surfaces. On the other hand, kinetic ions can enhance the coupling effect between the two rational surfaces when d_s is large. However, further investigations should be carried out to explore the physical dynamics of the interaction between kinetic ions and the DTMs.

It is known that the effect of kinetic ions includes the FLR effect and the effect of a finite radial magnetic drift (v_D) in a toroidal magnetic field. It has been found that the FLR effect is not important in the STM instability especially for large η [5,31] due to the fact that the ion gyro radius is much smaller than the width of the STM. The kinetic ions can affect the STM mainly through the magnetic drift in toroidal geometry. Since the width of the DTMs is much larger than that of the STM, we can speculate that the kinetic ions also affect the DTMs mainly through the magnetic drift. This can be illustrated by Table 1.

Table 1. FLR effect and magnetic drift effect on the DTMs growth rates for $\eta = 5\times10^{-5}$. The growth rates are normalized to the value from the cases with cold ions ($T_{0i} = 1\times10^{-3}$ keV).

	γ/γ_1
(1) $T_{0i} = 1\times10^{-3}$ keV, FLR = 1, $v_D = 1$	1.00
(2) $T_{0i} = 0.1$ keV, FLR = 0, $v_D = 0$	0.9932
(3) $T_{0i} = 0.1$ keV, FLR = 1, $v_D = 0$	0.9864
(4) $T_{0i} = 0.1$ keV, FLR = 1, $v_D = 1$	0.6254

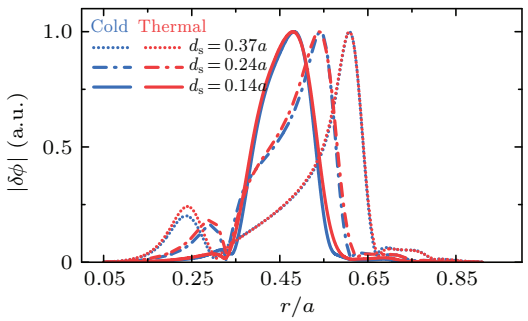


Fig. 9. The radial mode structures for $T_{0i} = 1\times10^{-3}$ keV and $T_{0i} = 0.1$ keV for $d_s = 0.37a$, $0.24a$, and $0.14a$. The profiles are normalized to their maximum absolute values.

It has been shown that the kinetic ions can provide either an energy source or sink for tearing modes.[17] To gain further

insight into the energy exchange between kinetic ions and the DTMs, the simulation results are studied by analyzing energy transfer between the ions and the wave field. Similar analysis has been given in our previous work for the STM.[5] Here we focus on the kinetic ion effect on the coupling of the two rational surfaces for the DTMs. A brief introduction to the numerical diagnostic of Joule heating is given in the following, and more details can be found in Ref. [5]. The energy-like equation can be derived as

$$\begin{aligned}\frac{\mathrm{d}E}{\mathrm{d}t} =& -\int \delta j_{\parallel \mathrm{i}} E_{\parallel}\,\mathrm{d}\boldsymbol{x} + \int \delta j_{\perp \mathrm{i}} \cdot \nabla\phi\,\mathrm{d}\boldsymbol{x} \\ & - \int e n_0 \delta u_{\parallel \mathrm{e}} E_{\parallel}\,\mathrm{d}\boldsymbol{x} + q_{\mathrm{i}} \int \phi \dot{n}_p\,\mathrm{d}\boldsymbol{x} \\ & + q_{\mathrm{i}} \int \phi \left(\frac{\partial \overline{\delta n_{\mathrm{i}}}}{\partial t}\right)_R \mathrm{d}\boldsymbol{x} - e \int \phi \left(\frac{\partial \delta n_{\mathrm{e}}}{\partial t}\right)_R \mathrm{d}\boldsymbol{x}, \quad (8)\end{aligned}$$

where $E = \frac{1}{2\beta_u}\int (\delta B_{\perp})^2 \mathrm{d}\boldsymbol{x}$ is the energy stored in the perturbed magnetic field. The main instability drive comes from the last term. The ion term proportional to $\left(\frac{\partial \overline{\delta n_{\mathrm{i}}}}{\partial t}\right)_R$ is negligible. The first four terms on the right side stand for the ions parallel joule heating ($\gamma_{\parallel \mathrm{i}}$), the ions perpendicular joule heating ($\gamma_{\perp \mathrm{i}}$), the electron parallel joule heating, and the energy spent on polarizing the ions, respectively. The contributions from trapped and passing ions are calculated separately.

As shown in Table 2, for thermal ions, both $\gamma_{\parallel \mathrm{i}}$ and $\gamma_{\perp \mathrm{i}}$ have dumping effect on the DTMs. The perpendicular Joule heating rate is larger than the parallel Joule heating rate for both trapped and passing ions. This is different from the STM result where the parallel Joule heating rate is dominant. The contribution of the passing ions to the damping rate is much larger than that of trapped ions in both the parallel and perpendicular directions.

In order to investigate the influence of kinetic ions on the coupling between the two rational surfaces, the radial distributions of ion Joule heating for different d_{s} are plotted in Fig. 10. It can be seen that the ion Joule heating rate is mainly distributed around the outer rational surface and the coupling region. For the distribution of $\gamma_{\parallel \mathrm{i}}$ (Fig. 10(a)), the peak on the right side of the outer rational surface decreases with the decrease of d_{s}, which means that the relative amplitude between the two rational surfaces is increased. For $\gamma_{\perp \mathrm{i}}$ (Fig. 10(b)), the damping rate can be significantly increased between the two rational surfaces and cause substantial damping of the DTMs as d_{s} is decreased. Therefore, one can conclude from the above observations that thermal ions can effectively impact the DTMs through the energy exchange between ions and wave fields around the outer rational surface and the coupling region. On the one hand, thermal ions can enhance the coupling effects of the DTMs. On the other hand, the enhanced coupling of the DTMs can in turn induce stronger energy exchange owing to the ion dynamics in the coupling region. The consequent result of such a wave-particle interaction is the suppression of the DTMs growth rate and extending of the resistivity scaling $\gamma \sim \eta^{1/3}$ to smaller η.

Table 2. The Joule heating rate of passing and trapped ions for $T_{0\mathrm{i}} = 10^{-3}$ keV and $T_{0\mathrm{i}} = 0.1$ keV when $\eta = 2\times10^{-5}$. The superscripts 'T' and 'P' represent trapped and passing ions, respectively; γ is the heating rate.

	$T_{0\mathrm{i}} = 1\times10^{-3}$ keV	$T_{0\mathrm{i}} = 0.1$ keV
$\gamma^{\mathrm{P}}_{\parallel \mathrm{i}}$	-5.05×10^{-5}	-6.75×10^{-5}
$\gamma^{\mathrm{T}}_{\parallel \mathrm{i}}$	-2.45×10^{-6}	-3.36×10^{-6}
$\gamma^{\mathrm{P}}_{\perp \mathrm{i}}$	0	-1.16×10^{-4}
$\gamma^{\mathrm{T}}_{\perp \mathrm{i}}$	0	-4.51×10^{-5}

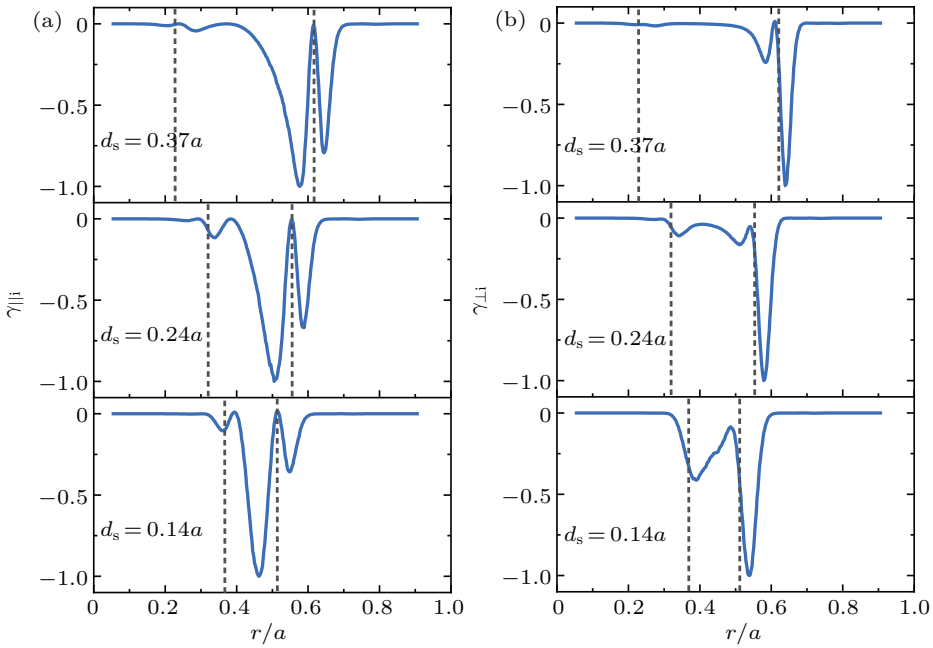


Fig. 10. Radial distributions of parallel (a) and perpendicular (b) ion Joule heating for $d_{\mathrm{s}} = 0.37a$, $d_{\mathrm{s}} = 0.24a$ and $d_{\mathrm{s}} = 0.14a$. All the profiles are normalized to the their maximum absolute values; $\gamma_{\perp \mathrm{i}}$ can be significantly increased between the two rational surfaces with decreasing d_{s} and can cause substantial damping for DTMs.

4. Conclusion

In this work, the effects kinetic ions on the linear DTMs are studied by using the GEM code with a gyrokinetic ion/fluid electron model. The toroidal effect can decrease the growth rate of the DTMs and increase the resistivity scaling for small η through the toroidal pressure term in the electron continuity equation. Thermal GK ions can decrease the growth rate of the DTMs significantly and change the resistivity scaling by enhancing the coupling effect of the two rational surfaces. The suppression effect increases with the ion temperature and the decrease of separation of the two rational surfaces. The mechanisms of the ions affecting the DTMs are studied through energy transfer analysis. It is found that the DTMs can be effectively affected by thermal ions through the energy exchange between ions and wave fields around the outer rational surface and the coupling region. Thermal ions can enhance the coupling effects of the DTMs. On the contrary, the enhanced coupling of the DTMs can in turn induce stronger energy exchange owing to the ion dynamics in the coupling region.

Acknowledgements

This work was supported by the National MCF Energy R&D Program of China (Grant No. 2019YFE03060001), the National Key R&D Program of China (Grant No. 2017YFE0300406), and the National Natural Science Foundation of China (Grant Nos. 11975272 and 11905257). Y. Chen is supported by the SciDAC Center Advanced Tokamak Modeling Environment (AToM) (Grant No. DE-SC0017992). The numerical calculations in this work were performed on the ShenMa High Performance Computing Cluster in Institute of Plasma Physics, Chinese Academy of Sciences, and resources of the National Energy Research Scientific Computing Center (NERSC), which are supported by the Office of Science of the U.S. Department of Energy (Grant No. DE-AC02-05CH11231).

References

[1] Pritchett P, Lee Y and Drake J 1980 *Phys. Fluids* **23** 1368
[2] Furth H, Rutherford P and Selberg H 1973 *Phys. Fluids* **16** 1054
[3] Chang Z, Park W, Fredrickson E, Batha S, Bell M, Bell R, Budny R, Bush C, Janos A, Levinton F, *et al.* 1996 *Phys. Rev. Lett.* **77** 3553
[4] Liu D, Zhang W, McClenaghan J, Wang J and Lin Z 2014 *Phys. Plasmas* **21** 122520
[5] Zhang R, Chen Y, Ye L and Xiang N 2022 *Phys. Plasmas* **29** 012108
[6] Wang J, Zheng-Xiong W, Lai W and Yue L 2017 *Nucl. Fusion* **57** 046007
[7] Ishii Y, Smolyakov A and Takechi M 2009 *Nucl. Fusion* **49** 085006
[8] Zhang R, Lu X, Huang Q, Dong J and Gong X 2016 *Phys. Plasmas* **23** 122509
[9] Wang Z X, Wei L, Wang X and Liu Y 2011 *Phys. Plasmas* **18** 050701
[10] Wang X Q, Wang X, Xu W B and Wang Z X 2011 *Phys. Plasmas* **18** 012102
[11] Zhang W, Ma Z and Wang S 2017 *Phys. Plasmas* **24** 102510
[12] Ye C, Wang Z X, Wei L and Hu Z Q 2019 *Nucl. Fusion* **59** 096044
[13] Sun G, Dong C and Duan L 2015 *Phys. Plasmas* **22** 092509
[14] Liu T, Wang Z X, Wang J and Wei L 2018 *Nucl. Fusion* **58** 076026
[15] Hazeltine R, Dobrott D and Wang T 1975 *Phys. Fluids* **18** 1778
[16] Drake J and Lee Y 1977 *Phys. Fluids* **20** 1341
[17] Cai H and Fu G 2012 *Phys. Plasmas* **19** 072506
[18] Rogers B, Kobayashi S, Ricci P, Dorland W, Drake J and Tatsuno T 2007 *Phys. Plasmas* **14** 092110
[19] Liu Y, Hastie R and Hender T 2012 *Phys. Plasmas* **19** 092510
[20] Hornsby W, Migliano P, Buchholz R, Kroenert L, Weikl A, Peeters A, Zarzoso D, Poli E and Casson F 2015 *Phys. Plasmas* **22** 022118
[21] Wang X Q and Wang X G 2016 *Nucl. Fusion* **57** 016039
[22] Gao B, Cai H, Wang F, Gao X and Wan Y 2021 *Phys. Plasmas* **28** 012104
[23] Yao Y, Lin Z, Dong J, Shi P, Liu S and Li J 2021 *Phys. Lett. A* **417** 127681
[24] Toi K, Takechi M, Takagi S, *et al.* 1999 *Nucl. Fusion* **39** 1929
[25] Shi P, Chen W, Wang Z, *et al.* 2021 *Nucl. Fusion* **61** 096025
[26] Chen Y and Parker S E 2007 *J. Comput. Phys.* **220** 839
[27] Chen Y and Parker S 2001 *Phys. Plasmas* **8** 441
[28] Chen Y and Parker S 2003 *J. Comput. Phys.* **189** 463
[29] Snyder P and Hammett G 2001 *Phys. Plasmas* **8** 3199
[30] Günter S, Schade S, Maraschek M, Pinches S, Strumberger E, Wolf R, Yu Q and Team A U 2000 *Nucl. Fusion* **40** 1541
[31] Chen Y, Chowdhury J, Parker S and Wan W 2015 *Phys. Plasmas* **22** 042111